American Journal of Biochemistry and Biotechnology

Original Research Paper

Thermodynamic Modeling and Heat-Moisture Transfer Characteristic Analysis of in Situ Thermal Desorption System for Polluted Soil

[1]Huijuan Xu, [2]Yanjun Bi, [1]Lijun Gao and [1]Dongxiao Ma

[1]Hebei Key Laboratory of Man-Machine Environmental Thermal Control Technology and Equipment, Hebei Vocational University of Technology and Engineering, China
[2]Department of Electrical Engineering, Hebei Vocational University of Technology and Engineering, China

Article history
Received: 18-04-2024
Revised: 12-06-2024
Accepted: 22-06-2024

Corresponding Author:
Dongxiao Ma
Hebei Key Laboratory of Man-machine Environmental Thermal Control Technology and Equipment, Hebei Vocational University of Technology and Engineering, China
E-mail: 13803199051@163.com

Abstract: In Situ Gas Thermal Desorption (ISGTD) is one of the effective approaches for organic contaminated soil. To investigate the heat-moisture transfer characteristics of soil during the heating process, a radially layered coupled heat-moisture model of the ISGTD system is established. The temperature and moisture distribution along the radial direction of the heat source, as well as the synergistic action of heat-moisture transfer at different heating stages are analyzed. The effects of heat intensity and initial water content on the heating performance are discussed. The results demonstrate that the liquid water migration driven by temperature gradient is greater than that driven by water content gradient and the liquid water migration in each soil unit increases from the heat-up stage to the superheating phase inside-out radially. The gas flow rate directly affects the stable temperature and heating time, while the initial water content only contributes to the heating time when the stable temperature remains unchanged. The correctness of the numerical model and results is verified by comparing them with on-site experimental data. Considering that high initial water content will lead to an extension of the heating time in the first two stages, further optimization design can be carried out for less gas flow rate and shorter heating time to achieve energy-saving remediation of high moisture soil. The above findings are of guiding significance in the engineering applications of contaminated soil remediation.

Keywords: Polluted Soil, Thermal Desorption, Dynamic Layered Model, Heat-Moisture Transfer

Introduction

Soil is an indispensable component of the ecological environment and the material basis of human social production and life. However, with accelerated global industrialization and urbanization, soil pollution has become an increasingly prominent concern, as has unreasonable industrial emissions, agricultural production and sewage irrigation (Khan *et al*., 2021). This phenomenon may directly change the intrinsic physical and chemical properties of soil, further leading to an imbalance in the ecological system. Even worse, the accumulated pollution in the soil can easily enter the food chain and seriously endangers the health of animals and human beings (Baltas *et al*., 2020; Khan *et al*., 2017; Zwolak *et al*., 2019). Given the universality and severity of soil contamination, the research on remediation technologies for contaminated soil has already become a hotspot. According to the nature of contaminants, soil pollution can be divided into organic pollution and inorganic pollution. The primary remediation technologies for organic pollution are physical remediation (such as excavation and Thermal Desorption, TD), chemical remediation (such as soil washing and oxidation-reduction technology), as well as biological remediation (Zheng *et al*., 2022; Sun *et al*., 2018). Excavation is mainly used for low-pollution soil. During excavation and transportation, volatile organic pollutants may cause air pollution. For soil washing and remediation, chemical eluents are easily adsorbed by soil to increase toxicity. Bio-remediation eliminates pollutants by decomposing contaminated substrates into nutrients, which requires a considerable period of time (Sun *et al*., 2018). Situ Thermal Desorption (ISTD) uses hot steam injection or heating elements to heat the soil to a sufficiently high temperature, separating organic

pollutants from the soil and collecting them for secondary treatment aboveground (Ding *et al*., 2019; Triplett *et al*., 2010). Compared with other technologies, ISTD has the advantages of no secondary pollution, high removal efficiency, short treatment period and recycling of soil. ISTD is suitable for the remediation of most volatile and semi-volatile organic pollutants, such as Petroleum HydroCarbons (PHCs), Polycyclic Aromatic Hydrocarbons (PAHs), PhthAlate Esters (PAEs), PolyChlorinated Biphenyls (PCBs), Hexa Chloro Benzenes (HCBs), Organo-Chlorine Pesticides (OCPs) and hexadecanes (Triplett *et al*., 2010; Kuppusamy *et al*., 2017; Zhao *et al*., 2019).

In the past few decades, ISTD has been successfully applied in many remediation projects, with an extremely high removal efficiency of organic contaminates (>99%) (EPA, 2017). In addition, ISTD is sustainable for land reuse. For construction land, most of the geotechnical properties increased after heating, indicating an improvement in the stability, bearing capacity and compressive strength of thermal repaired soil (Chen *et al*., 2018a). For agricultural land, heating below 250°C can increase nutrient availability and release dissolved organic carbon to support the growth of plants and microorganisms (Ding *et al*., 2019; Pape *et al*., 2015). However, heating above 250°C will reduce the content of organic matter and clay, damaging soil fertility (Ding *et al*., 2019; Pape *et al*., 2015). To restore ecological functions, further strategies are needed, such as adding soil nutrients and organic matter or mixing unpolluted soil with heated soil (Ding *et al*., 2019; Vidonish *et al*., 2016).

Since the removal of organic pollutants mainly depends on temperature, heating energy consumption is an important consideration factor. The energy used for heating can be electrical energy, natural gas combustion, or sustainable energy. Although the remediation cost mainly depends on the basic characteristics of contaminated soils (concentration of pollutants, moisture content and soil textural composition), ISTD is generally more expensive with an average cost of $76-$500 per metric ton treated (adjusted to 2024 USD) (Ding *et al*., 2019; Vidonish *et al*., 2016; Heron *et al*., 2009). To reduce energy consumption, (Xu *et al*., 2022) conducted numerical simulations to optimize the heating well arrangements. It is found that the triangular mode performs better than the hexagonal mode at the same well spacing and reducing the well spacing can improve the temperature uniformity of soil and reduce the overheating loss. Zhang *et al*. (2022) proposed three energy-saving strategies for an in-situ gas thermal remediation system and studied the natural gas consumption and energy utilization ratio. These studies mainly focus on improving the systematic design of ISTD to achieve energy saving and consumption reduction, with little consideration given to heat-mass transfer characteristics and their impact on the heating efficiency from the perspective of soil porous media characteristics.

Soil is a typical porous medium composed of three phases: Solid skeleton, liquid water and various gases. Essentially, the main process of thermal remediation is heat and mass transfer of multi-component and multi-phase flow in the porous media (De Vries, 1958; Nassar and Horton, 1997; Khan *et al*., 2021). For unsaturated soils with two forms of water in the pores (liquid water and gaseous water), this heat and mass transfer process is more complex. Specifically, moisture transfer in the unsaturated soil includes liquid water transfer driven by temperature gradient and water content gradient, as well as water vapor transfer under the action of temperature gradient and pressure gradient (Philip and De Vries, 1957; Cherati and Ghasemi-Fare, 2019). The above heat-moisture transfer process forms the distribution of temperature and moisture content in the soil (Hedayati-Dezfooli and Leong, 2019), greatly affecting the remediation efficiency and energy consumption of ISTD. It is of great significance to clarify the heat-mass transfer mechanisms and heating characteristics of soil during heat treatment and provide suggestions for effective heating strategies.

A radially layered coupled heat-moisture transfer model for unsaturated soil of an In Situ Gas Thermal Desorption (ISGTD) system is proposed to simulate the temperature and moisture distribution along the radial direction of the thermal well, as well as the synergistic effect of the heat-moisture transfer process in the heated soil. The system model is analyzed using numerical methods and validated using MATLAB. A detailed study is conducted on the spatial and temporal distribution of soil temperature and Volumetric Water Content (VWC) at different heating stages, as well as the heat-moisture transfer characteristics driven by temperature gradient and water content gradient. Meanwhile, the effect of natural gas flow and initial VWC on the thermal performance is studied respectively. The results can provide a theoretical reference for the design of heating strategies for energy-efficient ISTD applications.

Materials and Methods

System Description

The configuration of the ISGTD system for soil contamination is shown in Fig. (1). The system mainly consists of the burner, thermal well, polluted soil, extraction well and off-gas treatment unit. The heating gas generated by the combustion of natural gas and air in the burner flows into the thermal well, which is vertically inserted into the soil. As the heating gas flows in the thermal well, the restoration soil is heated to a sufficiently high temperature, allowing volatile contaminants to evaporate from the soil. This gaseous product is extracted from the extraction well and subjected to secondary treatment at the above ground to the off-gas treatment. In addition, to reduce heat dissipation and prevent pollutant diffusion during operation, an insulating layer is laid on the surface of the soil.

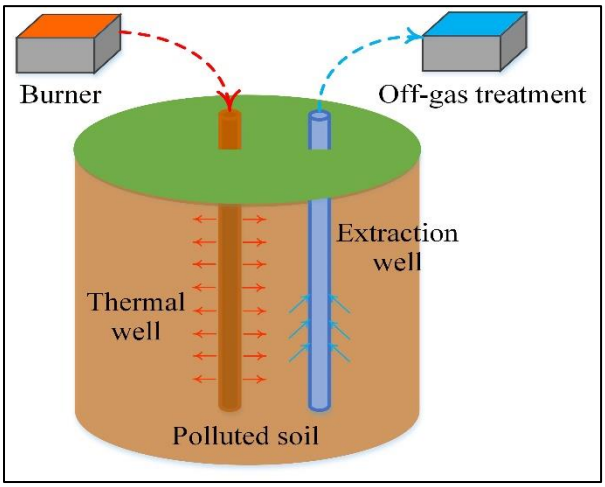

(a)

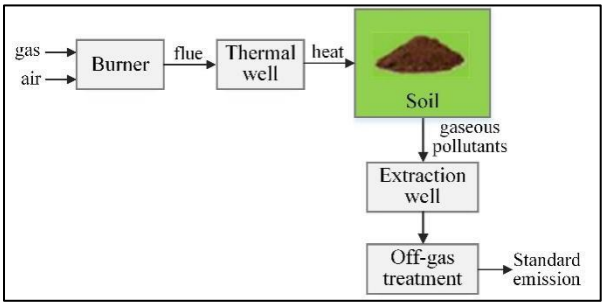

(b)

Fig. 1: System configuration of the ISGTD system; (a) Schematic diagram; (b) System flowchart

Based on the temperature variation of the heated soil (Zhang *et al*., 2022; Heron *et al*., 2015; 2013; 2009; Xu *et al*., 2020), the remediation process can be divided into the heat-up phase, boiling phase and superheating phase. In the heat-up phase (phase-1), the soil is heated from the initial temperature to 100°C In the boiling phase (phase-2), the temperature of the soil remains constant at 100°C with lots of liquid water evaporation. In the superheating phase (phase-3), the dry soil will be heated to a final high temperature with the organic contaminations evaporating from the soil.

There is coupling and mutual heat-moisture transfer in unsaturated soil during the thermal remediation process. The moisture transfer is mainly manifested by liquid water diffusion, liquid water evaporation and water vapor migration. During the heating process, the liquid water diffusion occurs within the target soil and between the target soil and the surrounding soil under combined temperature and moisture gradients. The transfer from liquid water to water vapor caused by evaporation only occurs in phase 2. The migration of water vapor under extraction occurs in phases 2 and 3. The first two moisture transfer processes are directly related to the heat transfer or temperature variation of the soil.

On the other side, the heat transfer in the soil is manifested in the following ways: Heat input caused by the migration of liquid water from the surrounding unheated sites; heat loss absorbed by liquid water evaporation; heat loss caused by extracting water vapor; heat input from the high-temperature flue gas of the thermal well in forms of heat conduction and heat convection; heat conduction between the heated soil and adjacent unheated sites as well as between the heated soil and the top insulation layer. The above heat-moisture transfer process plays a decisive role in the heating characteristics of the soil.

The physical model of the ISGTD system for simulation is shown in Fig. (2), which contains a burner, a heating well and the target soil with an insulation layer. There, a typical cylindrical soil unit with a heating well in the center is shown in Fig. (2a). It has an inner diameter of 1.45 m, an outer diameter of 4 m and a depth of 5.5 m. Figure (2b) shows the radially layered model of the heated site. To investigate the spatial distribution of soil temperature and moisture transfer along the radial direction of the heat source, the heating field is radially divided into 10 units on average, which are denoted as S_1, S_2, ... and S_{10}.

As shown in Fig. (2c), the burner, the thermal well and the layered soil units S_1, S_2, ... and S_{10} are respectively treated as lumped-parameter nodes based on the lumped-parameter method, detailed in section 2.2. For each layered unit of soil, S_n, the heat and mass inputs from adjacent layers, Γ_{n-1} and Γ_{n+1}, as well as the boundary conditions and initial conditions will determine the output characteristics of the target layer. They are mainly characterized by the temperature, stable temperature gradient, volumetric water content, liquid water migration, liquid water evaporation and heating time during the thermal desorption process. In addition, the determined conditions include the physical property parameters of the soil, such as initial temperature, initial volumetric water content, target heating temperature and conditions of top insulating and surrounding soil.

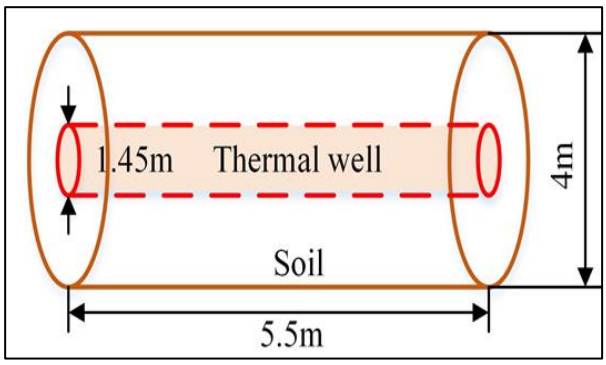

(a)

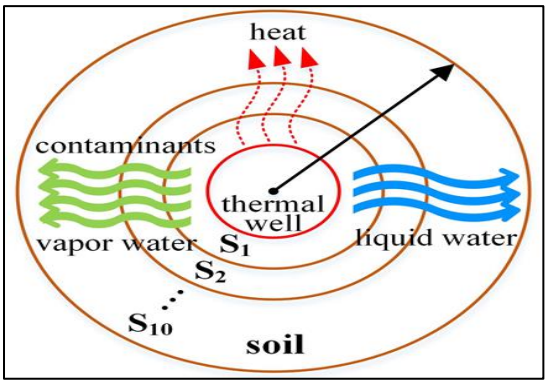

(b)

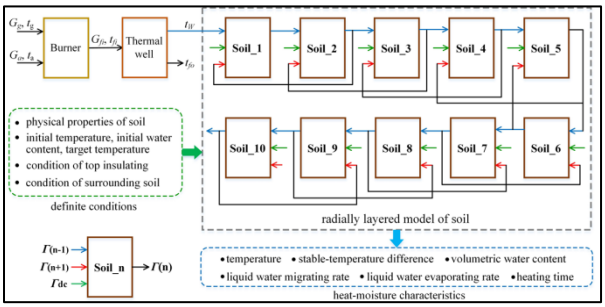

(c)

Fig. 2: Physical model of the system; (a) Longitudinal model of the heated unit; (b) Radially layered model of the heated site; (c) Lumped-parameter model of the system

Mathematical Modeling

The following assumptions are made in the model:

1. The soil is homogeneous and isotropic
2. The soil is unsaturated and consists of three phases: Gas, liquid and solid, which are all continuous
3. The air and water vapor in the soil are considered to be ideal gas
4. There is no heat-moisture transfer between the heated site and the surrounding sites at the boundary. The moisture transfer occurs between the heated soil and the underlying unheated soil
5. The pressure inside the soil is evenly distributed
6. The effects of organic pollutants on soil temperature are ignored as the impact of pollutants in soil is less than the orders of magnitude of water

Governing Equations of Mass Transfer

Based on the mass conservation principle, the variation of liquid water is equal to the difference between the amount of migration and the amount of inside evaporation. The liquid water migration in the unsaturated soil is primarily caused by the temperature gradient and the moisture gradient together based on Darcy's law (Bristow *et al.*, 1986; Santander and Bubnovich, 2002; Chen *et al.*, 2018b). Thus, the water content variation of each single soil unit, θ_{wn}, can be solved according to the following equations:

$$\rho_w V_{sn} \frac{d\theta_{wn}}{d\tau} = m_{wi\_n} - m_{wv\_n} \tag{1}$$

$$m_{wi\_n} = J_{wi\_n} A_{cs\_n} \tag{2}$$

$$\vec{J}_{wi\_n} = -\rho_w K_w (\nabla \psi_t) = -\rho_w \left(D_{wt} \frac{\partial t_{sn}}{\partial l} + D_{w\theta} \frac{\partial \theta_{wn}}{\partial l} - K_w \right) \tag{3}$$

where, ρ_w is the density of liquid water; V_{sn} is the volume of S_n; m_{wv_n} represents the mass of liquid water vaporized from S_n; m_{wi_n} denotes the mass of liquid water migrating into S_n; J_{wi_n} is liquid water migration flux density; t_{sn} is the temperature of S_n; D_{wt} and $D_{w\theta}$ are the mass diffusivities of the liquid water in soil caused by temperature gradient and moisture gradient respectively; l is the vertical transfer distance of the liquid water and K_w is the hydraulic conductivity of the soil.

The mass equation of vapor for S_n can be given as follows:

$$(\rho_v V_{sn}) \frac{d\theta_{vn}}{d\tau} = m_{wv\_n} - m_{vo\_n} \tag{4}$$

where, θ_{vn} is the vapor volumetric content of S_n; ρ_v is the density of vapor water; m_{vo_n} is the mass of vapor water extracted into the extraction well, calculated as follows:

$$m_{vo\_n} = \frac{N_e}{P_{eo} - P_{vn}} \cdot \frac{P_{vn}}{R_v T_{vn}} \tag{5}$$

where, N_e is the power of the extraction blower; P_{eo} is the outlet pressure of the extraction blower; R_v is the gas constant; P_{vn} is the pressure of the vapor water and T_{vn} is the Kelvin temperature of vapor water.

Governing Equations of Heat Transfer

According to the law of energy conservation, the energy change in the soil is equivalent to the sum of the heat generated by the thermal well, the heat flux caused by liquid migration and vapor migration, the energy absorbed by liquid water evaporation and the heat leakage at the top insulation layer and the lower unheated soil (Wang *et al.*, 2019). Therefore, the temperature dynamics of each single Soil unit (S_n) can be expressed as follows:

$$(m_{sn} c_s) \frac{dt_{sn}}{dt} = Q_{(n-1)(n)} - Q_{(n)(n+1)} + Q_{w\_n} - Q_{up\_n} - Q_{down\_n} - Q_{eva\_n} - Q_{v\_n} \tag{6}$$

where, m_{sn} and c_s are the mass of S_n and the mass-specific heat of the soil defined as follows:

$$m_s = \rho_{dry} \cdot (1-\varepsilon) \cdot V_s + \rho_w \cdot \theta_w \cdot V_s \quad (7)$$

$$c_m = \frac{0.85\rho_{dry} + 4200\theta_w}{\rho_{dry} + 1000\theta_w} \quad (8)$$

where, ρ_{dry} is the dry density of soil. $Q_{(n\text{-}1)(n)}$ is the heat conduction between S_n and $S_{n\text{-}1}$; $Q_{(n\text{-}1)(n)}$ is the heat conduction between S_n and S_{n+1}; Q_{up_n} and Q_{down_n} are the heat leakage between S_n and the top insulation layer, as well as that between S_n and the underlying unheated site; $Q_{(n\text{-}1)(n)}$ $Q_{(n)(n+1)}$ Q_{up_n} and Q_{down_n} can be calculated as follows:

$$\begin{cases} Q_{(n\text{-}1)(n)} = \dfrac{1}{R_{(n\text{-}1)(n)}}\left(t_{s(n\text{-}1)} - t_{sn}\right) \\ Q_{(n)(n+1)} = \dfrac{1}{R_{(n)(n+1)}}\left(t_{sn} - t_{s(n+1)}\right) \\ Q_{up\_n} = \dfrac{1}{R_{nu}}\left(t_{sn} - t_u\right) \\ Q_{down\_n} = \dfrac{1}{R_{nd}}\left(t_{sn} - t_d\right) \end{cases} \quad (9)$$

where, Q_{w_n} and Q_{v_n} indicate the migration heat of liquid water and extraction of vapor water respectively, calculated as follows:

$$\begin{cases} Q_{w\_n} = m_{wi\_n} h_w \\ Q_{v\_n} = m_{vo\_n} h_v \end{cases} \quad (10)$$

where, h_w and h_v are the specific enthalpy of liquid water and vapor water and m_{wi_n} and m_{vo_n} can be obtained by Eqs. (2) and (5).

Q_{eva_n} represents the energy absorbed by liquid water evaporation, calculated as follows:

$$Q_{eva\_n} = m_{wv\_n} H \quad (11)$$

where, H is the latent heat of water evaporation.

It is worth noting that when $n = 1$, the heat input $Q_{(n\text{-}1)(n)}$ in Eq. (6) should be replaced by $Q_{Ws,}$ which represents the heat conduction from the heating well to the innermost soil unit (S_1). Q_{Ws} can be described as follows:

$$Q_{Ws} = \frac{1}{R_{Ws}}\left(t_W - t_{s1}\right) \quad (12)$$

When $n = 10$, there is no heat conduction between the outermost soil unit and the surrounding block in line with assumption (4), that is, $Q_{(n)(n+1)} = 0$.

Simulation Condition Arrangement

System Parameters and Boundary Conditions

The above mathematical models are built and simulated in MATLAB R2017a. As the soil heating process is a slowly varying process, the sampling step is set as 3600 s (1 h) for simulation. Related parameter determinations of the ISGTD system are shown in Table 1.

The temperature of the top insulating layer and underlying unheated soil are 30 and 20°C respectively. Other parameters of the underlying unheated soil are consistent with those in Table 1. The power of the extraction pump is 5500 W. Based on assumption (4), there is no heat exchange between the heated soil and the boundary surrounding soil.

Simulation Cases

The heating temperature as well as the physical and chemical properties of soil is the primary factors affecting the thermal desorption efficiency. For the ISGTD system, the final heating temperature of the soil is mainly dependent on the heat supplied by the thermal well that is directly generated by the high-temperature flue gas of the burner. In addition, the initial water content of soil is an essential parameter affecting the thermal desorption effect and engineering cost. The variations of the mass flow rate of natural gas G_g and the volumetric water content of soil θ_{w0} are taken as two simulation conditions as shown in Table 2. Specifically, different disturbances in G_g and θ_{w0} are set to investigate the spatial and temporal distribution of temperature and moisture, as well as the synergistic action of the heat-moisture transfer process in the heated soil.

Table 1: Parameter determinations

Parameters	Values	Parameters	Values
Natural gas		Thermal well	
Density (kg/m^3)	0.728	Mass (kg)	1308.00
Specific heat (J·kg^{-1}·K^{-1})	34539.000	Specific heat (J·kg^{-1}·K^{-1})	472.00
Low heating value (J/m^3)	2185.000	Emissivity	0.35
Inlet temperature (°C)	20.000	black-body radiation coefficient (W·m^{-2}·K^{-4})	5.67
Air		Heat exchange efficiency	0.90
Density (kg/m^3)	1.029	Soil	
Specific heat (J·kg^{-1}·K^{-1})	1000.000	Dry density (kg/m^3)	1580.00
Inlet temperature (°C)	20.000	Density of liquid water (kg/m^3)	1000.00
Burner		Density of vapor water (kg/m^3)	0.60
Mass (kg)	25.026	Void ratio	0.35
Specific heat (J·kg^{-1}·K^{-1})	472.000	Initial temperature (°C)	20.00
Heat exchange efficiency	0.007	Latent heat of evaporation (J/kg)	2257200.00

Table 2: Arrangement of simulation cases

Simulation condition	Setting valueg/s	Simulation condition	Setting value m^3/m^3
The mass flow rate of	0.495	Initial volumetric water	0.15
natural gas	0.742	content of soil	0.20
	0.989		0.25
	1.237		0.30
	1.484		0.35

Results and Discussion

Steady-State Characteristics

In this section, the mass flow rate of natural Gas (G_g) and the initial volumetric water content (θ_{w0}) of soil are set as baseline values to analyze the steady-state characteristics. That is, G_g is 0.989 g/s and θ_{w0} is 0.25 m^3/m^3.

Figures 3(a-b) shows the variations of temperature and volumetric water content of different soil units S_1-$_{10}$. As shown in Fig. (3a), the variation tendency of t_{sn} is strictly consistent with the results (Xu *et al*., 2020; 2022; Li *et al*., 2019; Wang *et al*., 2019; Zhang *et al*., 2022; Heron *et al*., 2015). With continuous heating of the thermal well, t_{s1} firstly increases from 20-100°C within 0.6 days; and remains unchanged for 1.5 days due to the evaporation of liquid water. After all the liquid water of $S_1$is evaporated, t_{s1} continues to rise rapidly and is stable at 616°C within 66 days. With an inside-out process of heat transfer, t_{s2}-$_{s10}$ manifests the same rising characteristics as $t_{s1}$and then are stable together.

As shown in Fig. (3b), for phase-1, θ_{wn} is basically constant at 0.25 m^3/m^3. In phase 2, θ_{wn} declines considerably from 0.25-0 m^3/m^3 due to the large amount of liquid water evaporation. During phase 3, due to the extremely high temperature, the fluid water permeating from unheated areas will evaporate immediately and θ_{wn} remains constant at 0 m^3/m^3.

The heating time of three stages and stable temperature for S_1-$_{10}$ derived from Fig. (3a) are shown in Figs. (3c-d) respectively. The heating time of phase-1 ranges from 0.6-29.4 days, with increasing from S_1-$_{10}$ moderately. The heating time of phase 2 is concentrated within 1.5-4.6 days. The reason primarily lies in that the liquid water content in each unit increases gradually as the volume increases from S_1-$_{10}$. Compared with the first two stages, the heating time of phase 3 is 35-67 days. It is worth noting that since S_1 is the first to reach phase 3 and all units simultaneously reach the final stable state, the heating time of phase 3 decreases from S_1-$_{10}$.

The stable temperature of each unit (t_{sn_sta}) and the steady-state temperature difference between adjacent units (Δt_{sn_sta}) are respectively shown in Fig. (3d). It should be noted that t_{s1_sta} corresponding to S_1 denotes the steady-state temperature difference between the heating well and the innermost soil S_1. As shown in Fig. (3d), as the radial distance increases, t_{sn_sta} decreases successively from 616-524°C. These obvious temperature gradients are caused by the thermal resistance between adjacent layers. In addition, as the radial contact area of adjacent layers increases, the thermal resistance between the adjacent units decreases from S_1-$_{10}$ and the temperature gradient Δt_{sn_sta} also decreases.

Figure (3e) shows the variations of liquid water migration rate G_{wi} of different soil units during the heating process. According to Eq. (3), under the condition that the temperature and moisture content of the underlying soil are constant, the liquid water migration depends on the temperature of soil t_s, the volume moisture content of soil θ_w and the contact area between the heating field soil and the underlying soil. Since the liquid water migration caused by moisture gradient is far less than that caused by temperature gradients, the variation of G_{win} is basically similar to that of t_{sn} shown in Fig. (3a).

To further investigate the interaction between heat transfer and moisture transfer of the soil, the average value of water migration rate (G_{wi_a}) in each unit of the stages obtained from Fig. (3d) is shown in Fig. (3f). On the whole, G_{wi_a} gradually increases from S_1-$_{10}$ and increases from phases-1-3. Besides, G_{wi_a} of phase 3 is much larger than that of the first two stages. This can be explained as the contact area between the heated soil and the underlying unheated soil gradually increases from the inner unit (S_n) to the outer unit (S_{n+1}) and the temperature of different soil units increases from phases-1-3 state condition.

To verify the model, the findings are compared with other studies. The variations in soil temperature and VWC are strictly consistent with the results of numerous experimental studies (Sun *et al*., 2018; Ding *et al*., 2019; Triplett *et al*., 2010; Hedayati-Dezfooli and Leong, 2019; Heron *et al*., 2015; 2013; 2009; Xu *et al*., 2020). It has three distinct stages: The heat-up phase, boiling phase and superheating phase. The peak water content occurs in the outermost layer of soil at the end of phase 1. Regarding the study of heat-moisture transfer of unsaturated soil, (Chen *et al*., 2018b) pointed out that the peak water content was generated under the coupled effect of soil temperature gradient and water content gradient. Gao *et al*. (2020) found that the moisture migration flux was positively correlated with the temperature. These studies also strongly support the steady-state results shown in Fig. (3).

Dynamic Characteristics

The objective of this section is to analyze the effects of various input disturbances on the heat-moisture transfer characteristics of contaminated soil. For convenience, the soil units of S_1, S_5 and S_{10} are taken as main cases.

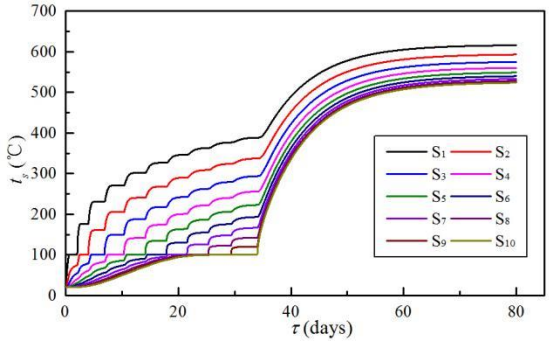

(a)

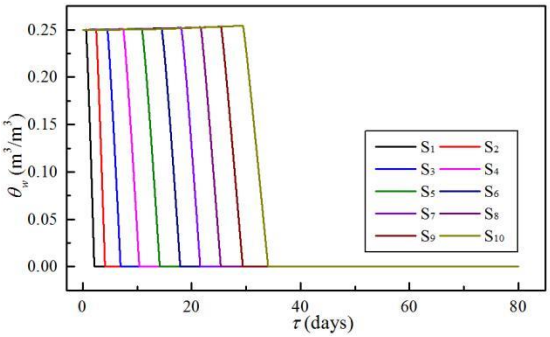

(b)

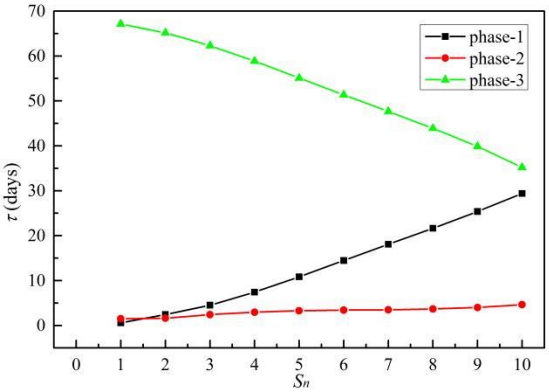

(c)

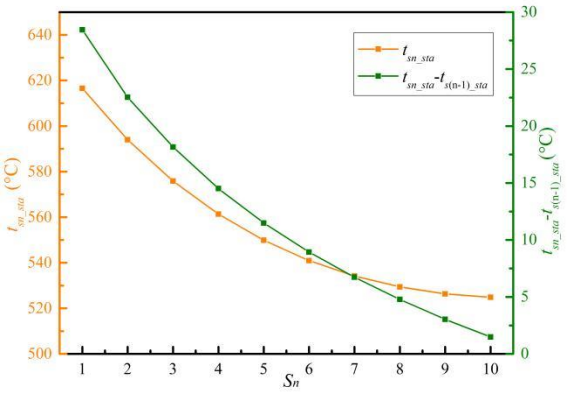

(d)

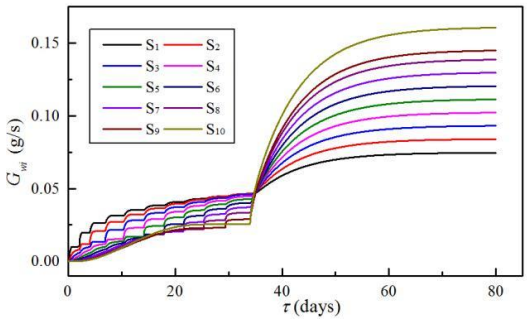

(e)

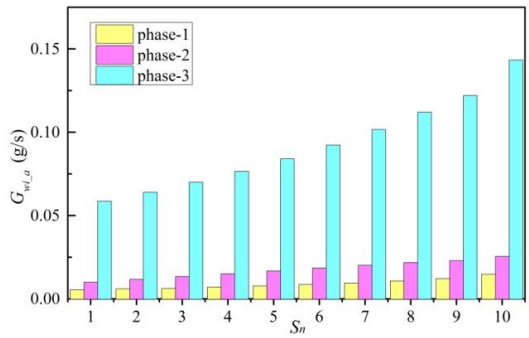

(f)

Fig. 3: Heating characteristics of the soil under steady-state conditions; (a) t_{sn} versus times; (b) θ_{wn} versus times; (c) The heating time of three stages; (d) The stable temperature and temperature difference of each unit; (e) Variations of G_{wi} of each unit; (f) G_{wi_a} of each unit

Disturbance of Natural Gas Mass Flow Rate

Figure 4 shows the temperature variations of the heated soil under different step disturbances in G_g as shown in Table 2. It can be seen that as G_g increases, the stable temperatures of all soil units increase exponentially. As S_5 shows, t_{s5_sta} increases from 376-640°C as G_g increases from -50% step-disturbance to +50% step-disturbance.

Figure 5 shows the heating time of three stages and the total heating time under different G_g. As the mass flow rate of natural gas increases, the heating power of the thermal well to the soil increases accordingly. Therefore, τ_1, τ_2 andτ_3 are all shortened and τ_1 and τ_3 are greatly affected. As shown in Fig. (5a), the closer to the radial outer units, the greater the effect of increased natural gas flow on the time required to reach a temperature of 100°C. When G_g increases from 0.495-1.484 g/s, τ_{1_s1} slightly decreases from 2.45-0.34 days; τ_{1_s5} decreases from 26.8-7.1 days significantly and τ_{1_s10} decreases more prominently from 61.8-21.4 days. For the boiling phase shown in Fig. (5b), as G_g increases, τ_{2_s1}, τ_{2_s5} and τ_{2_s10} are shortened by 4.3, 3.7 and 6.0 days respectively. For the superheating phase shown in Fig. (5c), as explained in section 3.1 in Fig. (3c), τ_3 shows a downtrend from S_1-$_{10}$ under the steady state. When G_g increases, τ_{3_s1}, τ_{3_s5} and τ_{3_s10} decrease by 58.6, 41.6 and 18.7 days respectively. As shown in Fig. (5), the

total heating time of the target soil decreases from 122.8-57.7 days as G_g increases.

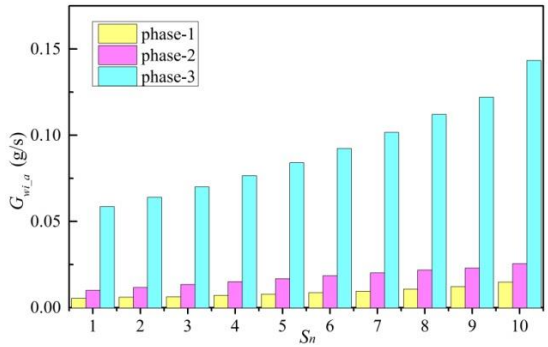

Fig. 4: Stable temperature of soil units at different G_g

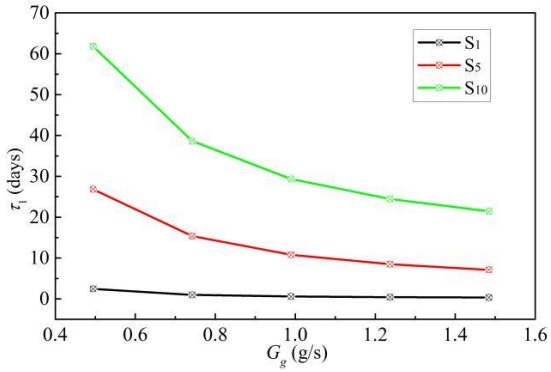

(a)

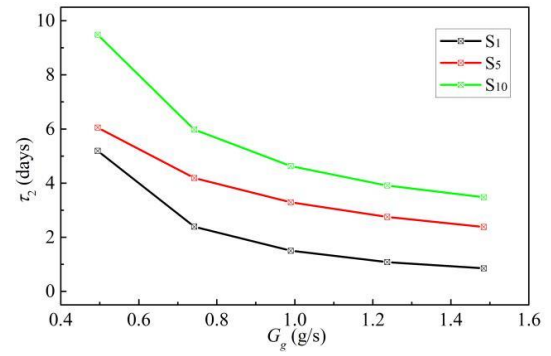

(b)

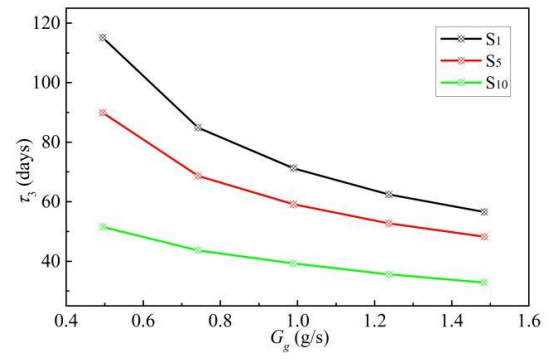

(c)

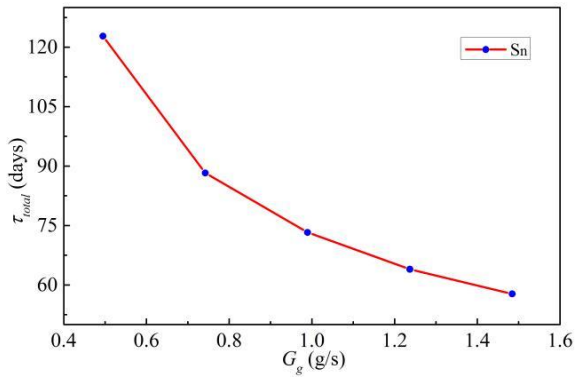

(d)

Fig. 5: The heating time at different G_g; (a) τ_1 under various G_g; (b) τ_2 at various G_g; (c) τ_3 versus G_g; (d) Total heating time under different G_g

The average value of water migration rate G_{wi_a} at different G_g is shown in Fig. (6). Consistent with the steady-state findings in Fig. (3c), G_{wi_a} of the outer unit (S_{n+1}) is larger than that of the inner unit (S_n) for any phases. Due to the shortening of τ_{1n} and the increment of volumetric water content decreases with the increment of G_g, G_{wi_a} of each soil unit slightly decreases in phase-1, as shown in Fig. (6a). In phase 2, as t_{sn} is constant at 100°C, G_{wi_a} of each soil unit is basically constant as shown in Fig. (6b). For phase-3 in Fig. (6c), G_{wi_a} of each soil unit shows an upward trend because that t_{sn} increases with the increase of G_g.

The heating power is the primary and critical factor that affects the heat-humidity characteristics and efficiency of ISTD (Zhao *et al*., 2019; Xu *et al*., 2020; Wang *et al*., 2019; Bulmău *et al*., 2014). For ISGTD, the natural gas flow rate determines the heating power to the soil. In another study of ISGTD (Zhao *et al*., 2019), increasing the gas flow rate would result in a fast temperature rising rate, high stable soil temperature (from 358-619°C) and decreased heating period (from 120.7-56.3 days). The above results are highly consistent with the dynamic characteristics of heat source disturbance in this section.

Disturbance of Initial Volumetric Water Content

The stable temperatures of S_1, S_5 and S_{10} under different disturbances of θ_{w0} correspond to the simulation in Table 2, as shown in Fig. 7. It can be seen that due to the variation in θ_{w0}, t_{s_sta} of each soil unit is invariable for constant G_g. $t_{s1\ sta}$, t_{s5_sta} and t_{s10_sta} are 620, 550 and 525°C respectively.

The heating time of the three stages and the total heating time under different θ_{w0} are shown in Fig. (8). It can be seen from Eqs. (7-8) that the changes in θ_{w0} will directly affect the mass of the soil (m_{sn}) and the specific heat of the soil (c_s). As θ_{w0} increases, MSN and c_s increase correspondingly, resulting in the increase of the heating time in phase-1 (τ_{1_n}) for all the soil units, as shown in Fig. (8a). Moreover, there is a linear relationship between τ_{1n} and θ_{w0}. The closer to the outer unit and the

greater the increment of heating time caused by the increase of $\theta_{w0}\tau_{1\_10}$ increases at a rate of 9.6 and τ_{1_1} increases at a rate of only 1.4 in proportion to θ_{w0}.

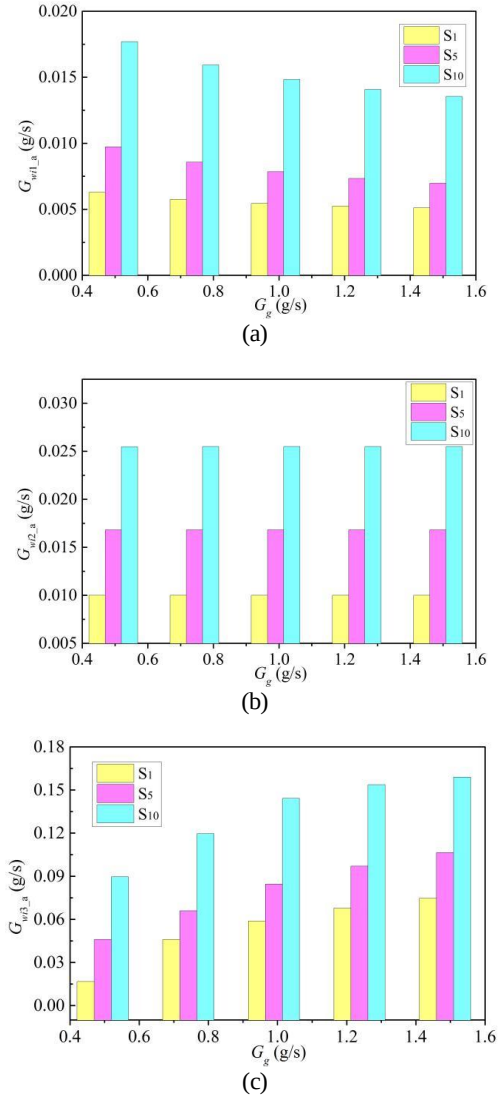

Fig. 6: The average value of water migration rate G_{wi_a} at different G_g; (a) G_{wi1_a} versus G_g; (b) G_{wi2_a} at various G_g; (c) G_{wi3_a} under different G_g

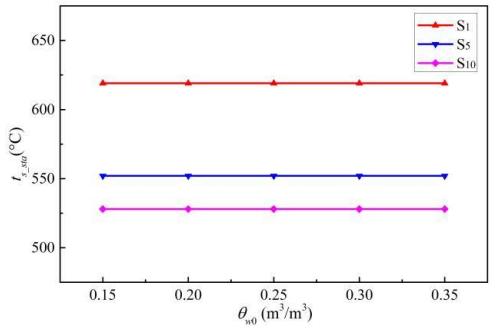

Fig. 7: The stable temperature of soil units with different θ_{w0}

For phase-2 shown in Fig. (8b), τ_{2_n} for $S_{1\text{-}10}$ also increases linearly as θ_{w0} increases. This can be attributed to that with a constant heating power, a larger θ_{w0} means more liquid water in the soil and a longer time for liquid water evaporation. When θ_{w0} increases from 0.15-0.35 m^3/m^3, τ_{2_1} increases linearly from 0.9-2.1 days with a slope of 5.6; τ_{2_5} increases from 2.1-4.4 days at a rate of 11.2 and τ_{2_10} increases from 2.9-6.3 days with a slope of 17.0. The settling time of the soil increases from 66.8-79.8 days in proportion to θ_{w0}, as shown in Fig. (8d).

The average value of water migration rate G_{wi_a} of the three stages under different θ_{w0} are shown in Fig. (9). Based on Eq. (3), the liquid water migration in the unsaturated soil is primarily caused by the temperature gradient and the moisture gradient. As θ_{w0} increases, G_{wi1} a increases slowly for all the soil units in phase-1 and phase-2 due to the increased moisture gradient and the steady temperature gradient. However, for phase 3 with continuous evaporation of the liquid water, the effect of moisture difference on the liquid water migration gradually decreases. Therefore, when θ_{w0} changes, G_{wi3} a remains constant for $S_{1\text{-}10}$. Usually, during the entire heating process, the liquid water migration of the radial outer soil unit is greater than that of the inner soil unit, which is completely consistent with the steady-state characteristics shown in Fig. (3f).

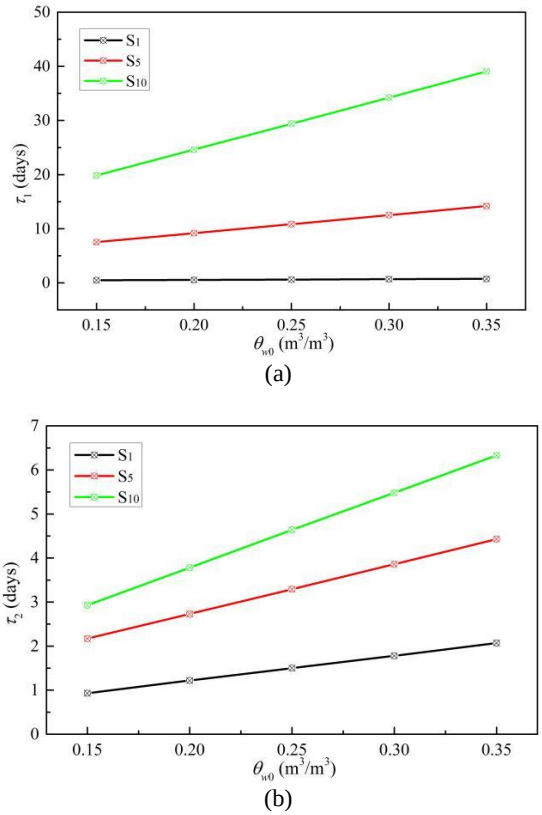

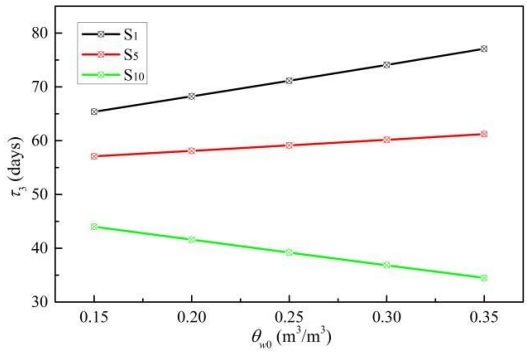

(c)

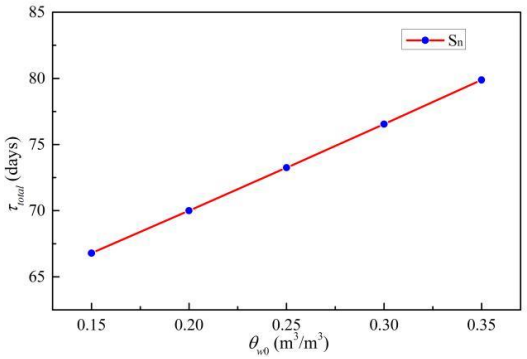

(d)

Fig. 8: Heating time of the three stages with different θ_{w0}; (a) τ_1 under various θ_{w0}; (b) τ_2 at various θ_{w0}; (c) τ_3 versus θ_{w0} (d) Total heating time under various θ_{w0}

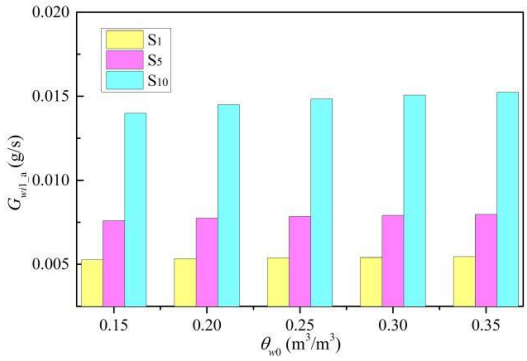

(a)

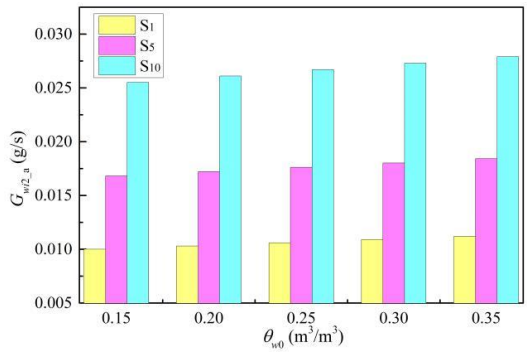

(b)

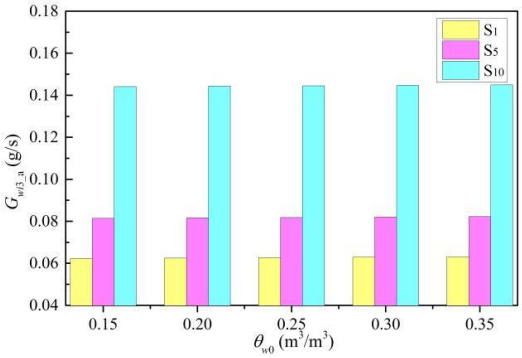

(c)

Fig. 9: Average value of water migration rate G_{wi_a} of the three stages with different θ_{w0}; (a) G_{wi1_a} versus θ_{w0}; (b) G_{wi2_a} at various θ_{w0}; (c) G_{wi3_a} under various θ_{w0}

Initial water content is another important influencing factor. Consistent with previous research (Zhao *et al*., 2019; Wang *et al*., 2019; Zhang *et al*., 2022), initial water content mainly influences the heat-up and boiling stages, especially the latter. As revealed by Wang *et al*. (2019), with initial water content increasing from 0.15-0.35 m^3/m^3, the boiling stage increased by 13 days. When the water content is high, water evaporation will increase the heat loss and increase the cost. In view of this problem, (Feeney *et al*., 1998) reported that the optimal water content of polluted soil for TD should be 0.1-0.2 m^3/m^3. Actually, many contaminated sites do not meet this condition. To balance high water content with low energy consumption, further research is needed to develop an energy-saving heating strategy at different stages by adapting the natural gas flow, rather than constant heat intensity during the entire heating process. Relevant research has been conducted by our team and will be published later.

Conclusion

In this study, the heat-moisture transfer characteristics of the soil in the ISGTD system are investigated with a radially layered model of the heated site. The main conclusions are summarized as follows:

1. The heat-moisture characteristics of soil show obvious temporal and spatial distributions during the TD process. With continuous heating, the temperature of soil increases gradually from the radial inner unit (S_n) to the outer unit (S_{n+1}) by stages and finally reaches a steady state with a temperature difference between adjacent units. The VWC of soil drops rapidly from S_1-$_{10}$ in phase 2. The liquid water migration rate in each unit increases from S_1-S_{10} and rises from phase-1-3
2. The natural gas flow has a major influence on the heat-moisture transfer characteristics of soil. As the natural gas flow rate increases, the stable temperature of each soil unit is markedly elevated, the settling time significantly increases and the migration rate of

liquid water slightly decreases in phase-1 and increases in phase-3

3. The initial water content of soil plays a prominent part in the settling time and moisture transfer but has no effect on the stable temperature of each soil unit. Moreover, the initial water content mainly influences the heat-up and boiling stages, especially the latter. The higher the initial water content, the greater the mass and mass-specific heat of the soil and the more liquid water evaporation, leading to a linear increase in heating time and energy consumption. In view of the thermal treatment of contaminated soil with high water content, future research should focus on an energy-saving heating strategy based on the impact of water content at different stages

Acknowledgment

This study was supported by Hebei Vocational University of Technology and Engineering and Xingtai science and Technology Bureau.

Funding Information

Funding for this study was provided by the key research and development project of Xingtai (no.2022zz054).

Author's Contributions

Huijuan Xu: Original draft writing, visualization, software development, validation, methodology, investigation and formal analysis.

Yanjun Bi: Writing review and editing, supervision, conceptualization and formal analysis.

Lijun Gao: Visualization, investigation, formal analysis, and data curation.

Dongxiao Ma: Writing review and editing, supervision, resources, methodology and conceptualization.

Ethics

The authors accept full responsibility for any ethical issues that may arise following the publication of this manuscript.

Conflict of Interest

The authors declare that they have no competing interests. The corresponding author affirms that all of the authors have read and approved the manuscript.

References

Baltas, H., Sirin, M., Gökbayrak, E., & Ozcelik, A. E. (2020). A case study on pollution and a human health risk assessment of heavy metals in agricultural soils around Sinop province, Turkey. *Chemosphere*, *241*, 125015. https://doi.org/10.1016/j.chemosphere.2019.125015

Bristow, K. L., Campbell, G. S., Papendick, R. I., & Elliott, L. F. (1986). Simulation of heat and moisture transfer through a surface residue soil system. *Agricultural and Forest Meteorology*, *36*(3), 193–214. https://doi.org/10.1016/0168-1923(86)90035-3

Bulmău, C., Mărculescu, C., Lu, S., & Qi, Z. (2014). Analysis of thermal processing applied to contaminated soil for organic pollutants removal. *Journal of Geochemical Exploration*, *147*, 298–305. https://doi.org/10.1016/j.gexplo.2014.08.005

Chen, X., Song, X., Lv, Z. Y., Ren, J. Q., Ding, D., Lin, N., Wei, C. L., & Fu, H. (2018a). Feasibility of thermal remediation of soil contaminated with PAHs. *Chinese Journal of Environmental Engineering*, *12*(10), 2833–2844. https://doi.org/10.12030/j.cjee.201804029

Chen, H., Chu, S., Luan, D., Li, Q., Zhang, L., & Zhai, H. (2018b). Performance study on heat and moisture transfer in soil heat charging. *International Journal of Sustainable Energy*, *37*(7), 669–683. https://doi.org/10.1080/14786451.2017.1323898

Cherati, D. Y., & Ghasemi-Fare, O. (2019). Analyzing transient heat and moisture transport surrounding a heat source in unsaturated porous media using the Green's function. *Geothermics*, *81*, 224–234. https://doi.org/10.1016/j.geothermics.2019.04.012

De Vries, D. A. (1958). Simultaneous transfer of heat and moisture in porous media. *Eos, Transactions American Geophysical Union*, *39*(5), 909–916. https://doi.org/10.1029/tr039i005p00909

Ding, D., Song, X., Wei, C., & LaChance, J. (2019). A review on the sustainability of thermal treatment for contaminated soils. *Environmental Pollution*, *253*, 449–463. https://doi.org/10.1016/j.envpol.2019.06.118

EPA. (2017). *Superfund Remedy Report* (United State Environmental Protection Agency). Office of Landand Emergency Management.

Feeney, R. J., Nicotri, P. J., & Janke, D. S. (1998). *Overview of Thermal Desorption Technology*. Defense Technical Information Center. https://doi.org/10.21236/ada352083

Gao, Y., Dong, S., Wang, C., Chen, Y., & Hu, W. (2020). Effect of thermal intensity and initial moisture content on heat and moisture transfer in unsaturated soil. *Sustainable Cities and Society*, *55*, 102069. https://doi.org/10.1016/j.scs.2020.102069

Hedayati-Dezfooli, M., & Leong, W. H. (2019). An experimental study of coupled heat and moisture transfer in soils at high temperature conditions for a medium coarse soil. *International Journal of Heat and Mass Transfer*, *137*, 372–389. https://doi.org/10.1016/j.ijheatmasstransfer.2019.03.131

Heron, G., Lachance, J., & Baker, R. (2013). Removal of PCE DNAPL from Tight Clays Using in Situ Thermal Desorption. *Groundwater Monitoring & Remediation*, *33*(4), 31–43. https://doi.org/10.1111/gwmr.12028

Heron, G., Parker, K., Fournier, S., Wood, P., Angyal, G., Levesque, J., & Villecca, R. (2015). World's Largest in Situ Thermal Desorption Project: Challenges and Solutions. *Groundwater Monitoring & Remediation*, *35*(3), 89–100. https://doi.org/10.1111/gwmr.12115

Heron, G., Parker, K., Galligan, J., & Holmes, T. C. (2009). Thermal Treatment of Eight CVOC Source Zones to Near Nondetect Concentrations. *Groundwater Monitoring & Remediation*, *29*(3), 56–65. https://doi.org/10.1111/j.1745-6592.2009.01247.x

Khan, M. A., Khan, S., Khan, A., & Alam, M. (2017). Soil contamination with cadmium, consequences and remediation using organic amendments. *Science of the Total Environment*, *601–602*, 1591–1605. https://doi.org/10.1016/j.scitotenv.2017.06.030

Khan, S., Naushad, Mu., Lima, E. C., Zhang, S., Shaheen, S. M., & Rinklebe, J. (2021). Global soil pollution by toxic elements: Current status and future perspectives on the risk assessment and remediation strategies A review. *Journal of Hazardous Materials*, *417*, 126039. https://doi.org/10.1016/j.jhazmat.2021.126039

Kuppusamy, S., Thavamani, P., Venkateswarlu, K., Lee, Y. B., Naidu, R., & Megharaj, M. (2017). Remediation approaches for Polycyclic Aromatic Hydrocarbons (PAHs) contaminated soils: Technological constraints, emerging trends and future directions. *Chemosphere*, *168*, 944–968. https://doi.org/10.1016/j.chemosphere.2016.10.115

Li, T.-T., Li, Y.-Z., Zhai, Z.-Z., Li, E.-H., & Li, T. (2019). Energy-Saving Strategies and their Energy Analysis and Exergy Analysis for In Situ Thermal Remediation System of Polluted-Soil. *Energies*, *12*(20), 4018. https://doi.org/10.3390/en12204018

Nassar, I. N., & Horton, R. (1997). Heat, Water and Solution Transfer in Unsaturated Porous Media: I - Theory Development and Transport Coefficient Evaluation. *Transport in Porous Media*, *27*(1), 17–38. https://doi.org/10.1023/a:1006583918576

Pape, A., Switzer, C., McCosh, N., & Knapp, C. W. (2015). Impacts of thermal and smouldering remediation on plant growth and soil ecology. *Geoderma*, *243–244*, 1–9. https://doi.org/10.1016/j.geoderma.2014.12.004

Philip, J. R., & De Vries, D. A. (1957). Moisture movement in porous materials under temperature gradients. *Eos, Transactions American Geophysical Union*, *38*(2), 222–232. https://doi.org/10.1029/tr038i002p00222

Santander, R. E., & Bubnovich, V. (2002). Assessment of Mass and Heat Transfer Mechanisms in Unsaturated Soil. *International Communications in Heat and Mass Transfer*, *29*(4), 531–545. https://doi.org/10.1016/s0735-1933(02)00350-0

Sun, J., Pan, L., Tsang, D. C. W., Zhan, Y., Zhu, L., & Li, X. (2018). Organic contamination and remediation in the agricultural soils of China: A critical review. *Science of the Total Environment*, *615*, 724–740. https://doi.org/10.1016/j.scitotenv.2017.09.271

Triplett, K., J. L., Dahlen, P. R., & Johnson, P. C. (2010). State-of-the-Practice Review of In Situ Thermal Technologies. *Groundwater Monitoring & Remediation*, *30*(4), 64–72. https://doi.org/10.1111/j.1745-6592.2010.01305.x

Vidonish, J. E., Zygourakis, K., Masiello, C. A., Sabadell, G., & Alvarez, P. J. J. (2016). Thermal Treatment of Hydrocarbon-Impacted Soils: A Review of Technology Innovation for Sustainable Remediation. *Engineering*, *2*(4), 426–437. https://doi.org/10.1016/j.eng.2016.04.005

Wang, W., Li, C., Li, Y.-Z., Yuan, M., & Li, T. (2019). Numerical Analysis of Heat Transfer Performance of In Situ Thermal Remediation of Large Polluted Soil Areas. *Energies*, *12*(24), 4622. https://doi.org/10.3390/en12244622

Xu, H.-J., Li, Y.-Z., Gao, L.-J., & Zhang, X. (2020). Planned Heating Control Strategy and Thermodynamic Modeling of a Natural Gas Thermal Desorption System for Contaminated Soil. *Energies*, *13*(3), 642. https://doi.org/10.3390/en13030642

Xu, X.-Y., Hu, N., Wang, Q., Fan, L.-W., & Song, X. (2022). A numerical study of optimizing the well spacing and heating power for in situ thermal remediation of organic-contaminated soil. *Case Studies in Thermal Engineering*, *33*, 101941. https://doi.org/10.1016/j.csite.2022.101941

Zhang, H., Zhang, X., Yin, Y., Liu, G., Zhu, Y., Tan, X., & Huang, Y. (2022). Comparison of Three Energy-Saving Strategies Based on Models Established for In Situ Gas Thermal Remediation of Contaminated Soil. *Geofluids*, *2022*, 1–12. https://doi.org/10.1155/2022/5447682

Zhao, C., Dong, Y., Feng, Y., Li, Y., & Dong, Y. (2019). Thermal desorption for remediation of contaminated soil: A review. *Chemosphere*, *221*, 841–855. https://doi.org/10.1016/j.chemosphere.2019.01.079

Zheng, W., Cui, T., & Li, H. (2022). Combined technologies for the remediation of soils contaminated by organic pollutants. A review. *Environmental Chemistry Letters*, *20*(3), 2043–2062. https://doi.org/10.1007/S10311-022-01407-Y

Zwolak, A., Sarzyńska, M., Szpyrka, E., & Stawarczyk, K. (2019). Sources of Soil Pollution by Heavy Metals and Their Accumulation in Vegetables: a Review. *Water, Air and Soil Pollution*, *230*(7). https://doi.org/10.1007/s11270-019-4221-y

Nomenclature

t Temperature (°C)
h specific enthalpy (kJ/kg)
m Mass (kg)
H Latent heat of evaporation (J/kg)
ρ Density (kg/m^3)Subscripts
s Volume (m^3)
s Soil
c Specific heat ($J \cdot kg^{-1} \cdot K^{-1}$)
w Liquid water
G Mass flow rate (g/s)
g Natural gas
P Pressure (Pa)
W Thermal well
R Thermal resistance (K/W)
sta Stable
θ Volumetric water content (m^3/m^3)
a Average
τ Time (days)
v Vapor water
ε Void ratio
0 Initial state
S Soil unit
n Radial layer

Abbreviation

ISGTD In situ gas thermal desorption
ISTD In situ thermal desorption
TD Thermal desorption
VWC Volumetric water content
PAHs Polycyclic aromatic hydrocarbons
PCBs Polychlorinated biphenyls
PHCs Petroleum hydrocarbons
HCBs Hexachlorobenzenes
OCPs Organo-chlorine pesticide